A new spectral method for numerical solution of the unbounded rough surface scattering problem

Ying He, Peijun Li [*],[1], Jie Shen [2]

Department of Mathematics, Purdue University, West Lafayette, IN 47907, United States

A R T I C L E   I N F O

A B S T R A C T

A new spectral method is developed to solve the unbounded rough surface scattering problem. An unbounded rough surface is referred to as a non-local perturbation of an infinite plane surface such that the whole rough surface lies within a finite distance of the original plane. The method uses a transformed field expansion to reduce the boundary value problem with a complex scattering surface into a successive sequence of transmission problems of a planar surface. Hermite orthonormal basis functions are adopted to further simplify these problems to fully decoupled one-dimensional two-point boundary value problems, which are solved efficiently by the Legendre–Galerkin method. Numerical results indicate that the method is efficient, accurate, and well-suited for solving the scattering problem by unbounded rough surfaces.

© 2014 Elsevier Inc. All rights reserved.

1. Introduction

The problems of acoustic and electromagnetic scattering by unbounded rough surfaces have received much attention from both the engineering and mathematical communities for their important applications in a wide range of scientific areas, such as modeling acoustic and electromagnetic wave propagation over outdoor ground and sea surfaces [29], optical scattering from the surface of materials in near-field optics or nano-optics [13], detection of underwater mines, especially those buried in soft sediments [34]. An unbounded rough surface is referred to as a non-local perturbation of an infinite plane surface such that the whole rough surface lies within a finite distance of the original plane. Due to the non-local perturbation, precise modeling and accurate computing present challenging mathematical and computational questions.

Mathematically, the well-posedness of the solution was studied in [9,10,12,22,25] for the acoustic wave scattering problem. In [24], a model problem was considered for the three-dimensional electromagnetic wave scattering by rough surfaces. The two-dimensional scalar model problem was also considered by integral equation methods in [8,11,15–17,36,37]. We refer to [7,30] for related scattering problems where weighted Sobolev spaces were considered for unbounded domains. In addition, the solutions are available by using approximate, asymptotic, or statistical methods in [14,19,29,31,34,35] and the references cited therein. Despite the large amount of work done so far, we are not aware of any efficient and accurate numerical method for solving the scattering problem by unbounded rough surfaces.
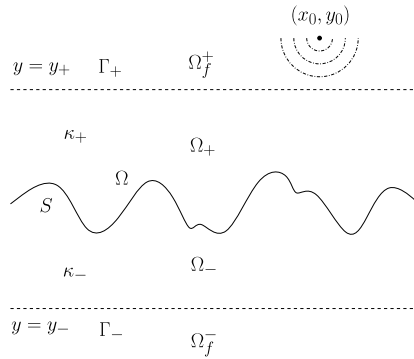
The present work is concerned with the numerical solution for such a scattering problem. We propose, as the first time, a new spectral method to rigorously solve the unbounded rough surface scattering problem. Specifically, we consider the

---

* Corresponding author.
E-mail addresses: he14@purdue.edu (Y. He), lipeijun@math.purdue.edu (P. Li), shen@math.purdue.edu (J. Shen).

Fig. 1. Problem geometry. A wave from the point source at (x_0, y_0) is incident on the scattering surface S from the top. The spaces Ω_f^+ (above S) and Ω_f^- (below S) are filled with materials whose wavenumbers are constants κ_+ and κ_-, respectively.

scattering of a time-harmonic wave field, which is generated from a point source and incident on an unbounded rough surface from the top. The spaces above and below the surface are filled with some homogeneous absorbing materials, which account for the dielectric permittivity with positive imaginary parts. The scattering phenomenon is modeled as a boundary value problem of the two-dimensional Helmholtz equation with transparent boundary conditions proposed on planar surfaces confining the surface. Under the assumption that the surface is a sufficiently small and smooth deformation of a planar surface, we use the transformed field expansion to reduce the two-dimensional Helmholtz equation with complex scattering surface into a successive sequence of the transmission problems with a planar interface. We adopt Hermite orthonormal basis functions to handle the difficulty from the infinite domain in horizontal direction, and further reduce the two-dimensional transmission problems into fully decoupled one-dimensional two-point boundary value problems, which are solved efficiently by the Legendre–Galerkin method. Numerical examples are reported for both the rough surface scattering problem and the plane surface scattering problem, where the analytic solution is available. Numerical errors are investigated for all the parameters such as the perturbation parameter and the wavenumbers, the truncation in the horizontal direction of the Hermite expansion and in the vertical direction of the Legendre expansion, and the transformed field power series expansion.

We refer to a series of papers [2–6,26] for the boundary perturbation methods for solving the diffraction grating problems. An improved boundary perturbation algorithm, termed as the transformed field expansion, was proposed in [27], where a change of variables was done first to flatten the scattering surface and then followed by the boundary perturbation technique. The transformed field expansion method was shown to be accurate, stable, and robust even at higher order [20,28] for solving the two- and three-dimensional bounded obstacle scattering problems. Recently, an efficient and stable spectral method was developed in [21] for the two-dimensional Helmholtz equation in a two-layered periodic structure, where a Legendre–Galerkin approximation was used to solve the reduced one-dimensional problems.

The outline of this paper is as follows. In Section 2, a model problem is introduced for scattering by an unbounded rough surface. Section 3 is devoted to the transformed field expansion. In Section 4, numerical approximations are considered for the reduced transmission problems. Numerical examples are presented to demonstrate the efficiency and accuracy of the proposed method in Section 5. The paper is concluded with some general remarks and directions for future research in Section 6.

2. Model problem

In this section, we shall introduce a mathematical model and define some notation for the unbounded rough surface scattering problem. As seen in Fig. 1, let the scattering surface be described by the curve

$$S = \{(x, y) : y = f(x), x \in \mathbb{R}\},$$

where f is a bounded and Lipschitz continuous function. The scattering surface S is embedded in the strip

$$\Omega = \{(x, y) \in \mathbb{R}^2 : y_- < y < y_+\} = \mathbb{R} \times (y_-, y_+),$$

where y_- is a negative constant and y_+ is a positive constant. Let $\Omega_f^+ = \{(x, y) : y > f(x)\}$ and $\Omega_f^- = \{(x, y) : y < f(x)\}$ be filled with materials whose wavenumbers are constants κ_+ and κ_-, respectively. In fact, the wavenumbers satisfy $\kappa_\pm^2 = \omega^2 \mu \varepsilon_\pm$, where ω is the angular frequency, μ is the magnetic permeability which is assumed to be a constant everywhere, and $\varepsilon_\pm$ are the electric permittivity in $\Omega_f^\pm$. In this work, the electric permittivity $\varepsilon_\pm$ are assumed to be two complex numbers with positive imaginary parts. The condition $\operatorname{Im} \kappa_\pm^2 > 0$ physically accounts for energy absorption and mathematically ensures the existence and uniqueness of the solution. Denote by $\Gamma_+ = \{y = y_+\}$ and $\Gamma_- = \{y = y_-\}$ the top and bottom boundaries of the domain Ω.

Suppose that a wave generated from a point source at (x_0, y_0) is incident on S from the top. Explicitly, the point incident field is taken as the fundamental solution of the Helmholtz equation in Ω_+, i.e.,

$$u^{\text{inc}}(x, y; x_0, y_0) = \frac{\text{i}}{4} H_0^{(1)}\big(\kappa_+ |(x, y) - (x_0, y_0)|\big), \tag{1}$$

where $H_0^{(1)}$ is the Hankel function of first kind with order zero, (x, y) is the observation point, and (x_0, y_0) is the given source point in Ω_+. Clearly the incident field satisfies the two-dimensional Helmholtz equation:

$$\Delta u^{\text{inc}}(x, y) + \kappa_+^2 u^{\text{inc}}(x, y) = -\delta(x - x_0)\delta(y - y_0) \quad \text{in } \mathbb{R}^2,$$

where δ is the Dirac delta function.

The scattering of time-harmonic electromagnetic waves in the transverse electric case can also be modeled by the two dimensional Helmholtz equation:

$$\Delta u(x, y) + \kappa^2 u(x, y) = -\delta(x - x_0)\delta(y - y_0) \quad \text{in } \mathbb{R}^2, \tag{2}$$

where the wavenumber

$$\kappa = \begin{cases} \kappa_+ & \text{in } \Omega_f^+, \\ \kappa_- & \text{in } \Omega_f^-. \end{cases}$$

Due to the unbounded scattering surface, the usual Sommerfeld radiation condition is no longer valid [1]. We insist that u is composed of bounded outgoing waves in Ω_+ and Ω_- plus the incident wave u^{inc} in Ω_+.

For any given u on $\Gamma_\pm$, define the boundary operators $T_\pm$:

$$T_\pm u = \frac{1}{\sqrt{2\pi}} \int_{\mathbb{R}} \pm \text{i}\beta_\pm \hat{u}(\xi, y_\pm) e^{\text{i}\xi x} d\xi,$$

where

$$\beta_\pm^2(\xi) = \kappa_\pm^2 - |\xi|^2 \quad \text{with } \text{Im}\,\beta_\pm(\xi) > 0.$$

Following [25], we can deduce transparent boundary conditions on $\Gamma_\pm$:

$$\partial_y u = T_\pm u + \rho^\pm \quad \text{on } \Gamma_\pm, \tag{3}$$

where

$$\rho^+ = \partial_y u^{\text{inc}} - T_+ u^{\text{inc}} \quad \text{and} \quad \rho^- = 0. \tag{4}$$

Next we reformulate the scattering problem (2) and (3) into a transmission problem which is convenient to introduce the transformed field expansion [27].

Denote $\Omega_\pm = \Omega_f^\pm \cap \Omega$, as seen in Fig. 1. Consider the Helmholtz equation (2) in $\Omega_\pm$:

$$\Delta u^\pm + \kappa_\pm^2 u^\pm = 0 \quad \text{in } \Omega_\pm. \tag{5}$$

Recall the non-local transparent boundary conditions (3)

$$\partial_y u^\pm = T_\pm u^\pm + \rho^\pm \quad \text{on } \Gamma_\pm. \tag{6}$$

Following from the jump conditions, we obtain that the field and its normal derivative are continuous across S, i.e.,

$$u^+\big(x, f(x)\big) = u^-\big(x, f(x)\big), \tag{7}$$

$$\partial_{\mathbf{n}} u^+\big(x, f(x)\big) = \partial_{\mathbf{n}} u^-\big(x, f(x)\big), \tag{8}$$

where $\mathbf{n} = (n_1, n_2)^\top$ is the unit normal vector pointing from Ω_+ to Ω_-. Explicitly, we have

$$n_1 = \frac{f'(x)}{\sqrt{1 + [f'(x)]^2}} \quad \text{and} \quad n_2 = -\frac{1}{\sqrt{1 + [f'(x)]^2}}.$$

Hence, the transmission problem is to find the fields u^+ and u^-, which satisfy the Helmholtz equation (5), the boundary condition (6), and the continuity conditions (7) and (8). It was shown in [25] that the transmission problem has a unique weak solution; furthermore, an analytic solution was deduced as an infinite series under the assumption that the scattering surface S is a sufficiently small and smooth deformation of a plane surface.

3. Transformed field expansion

The transformed field expansion method begins with the change of variables:

$$x_1 = x, \qquad y_1 = y_+ \left(\frac{y - f}{y_+ - f} \right), \quad f < y < y_+,$$

and

$$x_2 = x, \qquad y_2 = y_- \left(\frac{y - f}{y_- - f} \right), \quad y_- < y < f,$$

which maps the domains Ω_+ and Ω_- to the rectangular domains $D_+ = \{(x, y) \in \mathbb{R}^2 : 0 < y < y_+\}$ and $D_- = \{(x, y) \in \mathbb{R}^2 : y_- < y < 0\}$, respectively.

It is easy to verify the differentiation rules

$$\partial_x = \partial_{x_1} - f' \left(\frac{y_+ - y_1}{y_+ - f} \right) \partial_{y_1},$$

$$\partial_y = \left(\frac{y_+}{y_+ - f} \right) \partial_{y_1},$$

for $f < y < y_+$, and

$$\partial_x = \partial_{x_2} - f' \left(\frac{y_- - y_2}{y_- - f} \right) \partial_{y_2},$$

$$\partial_y = \left(\frac{y_-}{y_- - f} \right) \partial_{y_2},$$

for $y_- < y < f$.

Introduce new functions $w^+(x_1, y_1) = u^+(x, y)$ and $w^-(x_2, y_2) = u^-(x, y)$ under the transformation. It can be verified after tedious but straightforward calculations that $w^\pm$, upon dropping the subscript, satisfy the equation

$$c_1^\pm \frac{\partial^2 w^\pm}{\partial x^2} + c_2^\pm \frac{\partial^2 w^\pm}{\partial y^2} + c_3^\pm \frac{\partial^2 w^\pm}{\partial x \partial y} + c_4^\pm \frac{\partial w^\pm}{\partial y} + c_1^\pm \kappa_\pm^2 w^\pm = 0 \quad \text{in } D_\pm, \tag{9}$$

where

$$c_1^\pm = (y_\pm - f)^2,$$
$$c_2^\pm = \left[f'(y_\pm - y) \right]^2 + y_+^2,$$
$$c_3^\pm = -2 f'(y_\pm - y)(y_\pm - f),$$
$$c_4^\pm = -(y_\pm - y) \left[f''(y_\pm - f) + 2 (f')^2 \right].$$

The non-local transparent boundary conditions (6) are

$$\partial_y w^\pm = \left(1 - \frac{f}{y_\pm} \right) (T_\pm w^\pm + \rho^\pm) \quad \text{on } \Gamma_\pm. \tag{10}$$

The continuity conditions (7) and (8) reduce to

$$w^+(x, 0) = w^-(x, 0), \tag{11}$$

$$\left(\frac{y_+}{y_+ - f} \right) \partial_y w^+(x, 0) = \left(\frac{y_-}{y_- - f} \right) \partial_y w^-(x, 0). \tag{12}$$

We assume that the scattering surface S is a sufficiently small perturbation of the flat plane, i.e., $f = \varepsilon g$ with ε sufficiently small comparing with the wavelength of the incident field. We consider the formal expansions of $w^\pm$ in a power series of ε:

$$w^\pm(x, y; \varepsilon) = \sum_{k=0}^\infty w_k^\pm(x, y) \varepsilon^k. \tag{13}$$

Substituting $f = \varepsilon g$ into $c_j^\pm$ and inserting the above expansions into (9), we may derive the recursions for $w_k^\pm$:

$$\frac{\partial^2 w_k^\pm}{\partial x^2} + \frac{\partial^2 w_k^\pm}{\partial y^2} + \kappa_\pm^2 w_k^\pm = v_k^\pm \quad \text{in } D_\pm, \tag{14}$$

where

$$
\begin{aligned}
v_k^\pm = {} & \frac{2g}{y_\pm}\frac{\partial^2 w_{k-1}^\pm}{\partial x^2} + \frac{2g'(y_\pm - y)}{y_\pm}\frac{\partial^2 w_{k-1}^\pm}{\partial x \partial y} + \frac{g''(y_\pm - y)}{y_\pm}\frac{\partial w_{k-1}^\pm}{\partial y} + \frac{2\kappa_\pm^2 g}{y_\pm}w_{k-1}^\pm \\
& - \frac{g^2}{y_\pm^2}\frac{\partial^2 w_{k-2}^\pm}{\partial x^2} - \frac{(g')^2(y_\pm - y)^2}{y_\pm^2}\frac{\partial^2 w_{k-2}^\pm}{\partial y^2} - \frac{2gg'(y_\pm - y)}{y_\pm^2}\frac{\partial^2 w_{k-2}^\pm}{\partial x \partial y} \\
& + \frac{[2(g')^2 - gg''](y_\pm - y)}{y_\pm^2}\frac{\partial w_{k-2}^\pm}{\partial y} - \frac{\kappa_\pm^2 g^2}{y_\pm^2}w_{k-2}^\pm.
\end{aligned}
$$

The non-local boundary conditions (10) become

$$
\partial_y w_k^\pm - T_\pm w_k^\pm = \rho_k^\pm, \quad y = y_\pm, \tag{15}
$$

where

$$
\rho_0^+ = \rho, \qquad \rho_1^+ = -\left(\frac{g}{y_+}\right)T_+ w_0^+ - \left(\frac{g}{y_+}\right)\rho, \qquad \rho_k^+ = -\left(\frac{g}{y_+}\right)T_+ w_{k-1}^+, \quad k = 2, 3, \ldots,
$$

$$
\rho_0^- = 0, \qquad \rho_k^- = \left(\frac{g}{y_-}\right)T_- w_{k-1}^-, \quad k = 1, 2, \ldots.
$$

The continuity conditions (11) and (12) at the interface $y = 0$ reduce to

$$
w_k^+(x, 0) - w_k^-(x, 0) = 0, \tag{16}
$$

$$
\partial_y w_k^+(x, 0) - \partial_y w_k^-(x, 0) = h_k, \tag{17}
$$

where

$$
h_0 = 0, \qquad h_k = \left(\frac{g}{y_-}\right)\partial_y w_{k-1}^+ - \left(\frac{g}{y_+}\right)\partial_y w_{k-1}^-, \quad k = 1, 2, \ldots.
$$

We notice that the Helmholtz problem (14) for the current terms $w_k^\pm$ involve some non-homogeneous terms $v_k^\pm$, $\rho_k^\pm$, and h_k, which only depend on previous two terms $w_{k-1}^\pm$ and $w_{k-2}^\pm$. Thus, the transmission problem (14)–(17) in rectangular domains $D_\pm$ indeed can be solved efficiently in a recursive manner starting from $k = 0$.

When solving the transmission problem (14)–(17) numerically, a main difficulty is how to treat the non-local boundary conditions (15). It is shown in [25] that the boundary conditions (15) become *local* in the frequency space after taking the Fourier transform in x. Indeed, dropping the subscript k for simplicity of notation and taking the Fourier transform of (14) with respect to the variable x, we obtain

$$
\frac{\partial^2 \hat{w}^\pm}{\partial y^2} + \left(\kappa_\pm^2 - \xi^2\right)\hat{w}^\pm = \hat{v}^\pm. \tag{18}
$$

The non-local boundary conditions (15) become:

$$
\partial_y \hat{w}^\pm \mp i\beta_\pm \hat{w}^\pm = \hat{\rho}^\pm, \tag{19}
$$

which is local in the Fourier variable ξ. The continuity conditions reduce to

$$
\hat{w}^+(\xi, 0) - \hat{w}^-(\xi, 0) = 0, \tag{20}
$$

$$
\partial_y \hat{w}^+(\xi, 0) - \partial_y \hat{w}^-(\xi, 0) = \hat{h}. \tag{21}
$$

We observe that for each $\xi \in \mathbb{R}$, the problem (18)–(21) is a one-dimensional two-point boundary value problem whose solution can expressed analytically [25]. However, these analytic expressions are of limited use in practice, since the solution is expressed in the Fourier variable ξ which cannot readily converted to the physical variable x due to the lack of discrete Fourier transform in $\mathbb{R}$. In the next section, we use orthonormal Hermite basis functions which play the role of the Fourier transform numerically and allow us to reduce the two-dimensional problem (14)–(17) into a sequence of one-dimensional problems that can be solved efficiently and accurately by a Legendre–Galerkin method.

4. Approximation

In this section, we consider an approximation to the transmission problem (18)–(21) by using the Hermite orthonormal functions for the horizontal x-direction and the Legendre–Galerkin method for the reduced one-dimensional problem in the vertical y-direction.

4.1. Hermite orthonormal basis

Denote by $H_m(x)$ the Hermite polynomial of degree m on $\mathbb{R}$ for $m = 0, 1, 2, \cdots$. These polynomials are orthogonal with respect to the weigh function e^{-x^2}, i.e.,

$$\int_{\mathbb{R}} H_m(x)H_k(x)e^{-x^2}\,dx = 2^m m! \sqrt{\pi}\delta_{mk}, \tag{22}$$

where δ_{mk} is the Dirac delta function. The sequence of Hermite polynomials satisfies the recursion

$$H_{m+1}(x) = 2xH_m(x) - 2mH_{m-1}(x) \tag{23}$$

and the identity

$$H'_m(x) = 2mH_{m-1}(x). \tag{24}$$

Define a sequence of Hermite functions

$$\psi_m(x) = \left(2^m m!\sqrt{\pi}\right)^{-1/2} H_m(x)e^{-x^2/2}.$$

It follows from (22) that the Hermite functions form an orthonormal basis of the Hilbert space $L^2(\mathbb{R})$, i.e.,

$$\int_{\mathbb{R}} \psi_m(x)\psi_k(x)\,dx = \delta_{mk}. \tag{25}$$

Furthermore, they satisfy the recursion

$$\psi_{m+1}(x) = \sqrt{\frac{2}{m+1}}x\psi_m(x) - \sqrt{\frac{m}{m+1}}\psi_{m-1}(x) \tag{26}$$

and the identity

$$\psi'_m(x) = -x\psi_m(x) + \sqrt{2m}\psi_{m-1}(x). \tag{27}$$

The following result plays a key role in our algorithm. We refer to [18] (cf. page 22) for the proof.

Lemma 4.1. *The Hermite function ψ_m is the eigenfunction of the Fourier transform operator with eigenvalue $(-i)^m$, $m = 0, 1, \ldots$, i.e.,*

$$\hat{\psi}_m(\xi) = \frac{1}{\sqrt{2\pi}}\int_{\mathbb{R}} \psi_m(x)e^{-i\xi x}\,dx = (-i)^m\psi_m(\xi).$$

Using the Hermite basis functions, we consider the expansions

$$w^{\pm}(x, y) = \sum_{m=0}^{\infty} w_m^{\pm}(y)\psi_m(x),$$

$$v^{\pm}(x, y) = \sum_{m=0}^{\infty} v_m^{\pm}(y)\psi_m(x),$$

$$\rho^{\pm}(x) = \sum_{m=0}^{\infty} \rho_m^{\pm}\psi_m(x),$$

$$h(x) = \sum_{m=0}^{\infty} h_m\psi_m(x).$$

Taking the Fourier transform with respect to x of the above expansions and using Lemma 4.1, we have

$$\hat{w}^{\pm}(\xi, y) = \sum_{m=0}^{\infty} (-i)^m w_m^{\pm}(y)\psi_m(\xi),$$

$$\hat{v}^{\pm}(\xi, y) = \sum_{m=0}^{\infty} (-i)^m v_m^{\pm}(y)\psi_m(\xi),$$

$$\hat{\rho}^{\pm}(\xi) = \sum_{m=0}^{\infty} (-i)^m \rho_m^{\pm}\psi_m(\xi),$$

$$\hat{h}(\xi) = \sum_{m=0}^{\infty} (-i)^m h_m\psi_m(\xi).$$

Plugging the above expansions into (18) yields

$$\sum_{m=0}^{\infty}\left[(-\mathrm{i})^m\frac{\mathrm{d}^2w_m^{\pm}(y)}{\mathrm{d}y^2}\psi_m(\xi)+(-\mathrm{i})^m\left(\kappa_{\pm}^2-\xi^2\right)w_m^{\pm}(y)\psi_m(\xi)\right]=\sum_{m=0}^{\infty}(-\mathrm{i})^mv_m^{\pm}(y)\psi_m(\xi). \tag{28}$$

The boundary condition (19) reduce to

$$\sum_{m=0}^{\infty}\left[(-\mathrm{i})^m\frac{\mathrm{d}w_m^{\pm}(y_{\pm})}{\mathrm{d}y}\psi_m(\xi)\mp(-\mathrm{i})^m\mathrm{i}\beta_{\pm}w_m^{\pm}(y_{\pm})\psi_m(\xi)\right]=\sum_{m=0}^{\infty}(-\mathrm{i})^m\rho_m^{\pm}\psi_m(\xi). \tag{29}$$

The continuity conditions (20) and (21) reduce to

$$\sum_{m=0}^{\infty}(-\mathrm{i})^m\left[w_m^+(0)-w_m^-(0)\right]\psi_m(\xi)=0, \tag{30}$$

and

$$\sum_{m=0}^{\infty}(-\mathrm{i})^m\left[\frac{\mathrm{d}w_m^+(0)}{\mathrm{d}y}-\frac{\mathrm{d}w_m^-(0)}{\mathrm{d}y}\right]\psi_m(\xi)=\sum_{m=0}^{\infty}(-\mathrm{i})^mh_m\psi_m(\xi). \tag{31}$$

Define a diagonal matrix

$$D=\mathrm{diag}\left((-\mathrm{i})^0,(-\mathrm{i})^1,(-\mathrm{i})^2,\ldots,(-\mathrm{i})^m,\ldots\right)$$

and vectors

$$\mathbf{w}^{\pm}(y)=D\cdot\left(w_0^{\pm}(y),w_1^{\pm}(y),\ldots,w_m^{\pm}(y),\ldots\right)^{\top},$$
$$\mathbf{v}^{\pm}(y)=D\cdot\left(v_0^{\pm}(y),v_1^{\pm}(y),\ldots,v_m^{\pm}(y),\ldots\right)^{\top},$$
$$\boldsymbol{\rho}^{\pm}=D\cdot\left(\rho_0^{\pm},\rho_1^{\pm},\ldots,\rho_m^{\pm},\ldots\right)^{\top},$$
$$\mathbf{h}=D\cdot\left(h_1,h_2,\ldots,h_m,\ldots\right)^{\top}.$$

Define matrices $A=(a_{ij})$ and $S^{\pm}=(s_{ij}^{\pm})$ with entries given by

$$a_{ij}=\int_{\mathbb{R}}\xi^2\psi_j(\xi)\psi_i(\xi)\mathrm{d}\xi$$

and

$$s_{ij}^{\pm}=\int_{\mathbb{R}}\pm\mathrm{i}\beta_{\pm}\psi_j(\xi)\psi_i(\xi)\mathrm{d}\xi.$$

It can be easily verified from (25) and (26) that the matrix A is symmetric and tri-diagonal with entry given by

$$a_{ij}=\frac{\sqrt{(i+1)(j+1)}+\sqrt{ij}}{2}\delta_{i,j}+\frac{\sqrt{(i+1)j}}{2}\delta_{i+1,j-1}+\frac{\sqrt{i(j+1)}}{2}\delta_{i-1,j+1}.$$

Multiplying the Hermite basis function and integrating in $\mathbb{R}$, we may rewrite (28) into the matrix form:

$$\frac{\mathrm{d}^2\mathbf{w}^{\pm}(y)}{\mathrm{d}y^2}+\left(\kappa_{\pm}^2I-A\right)\mathbf{w}^{\pm}(y)=\mathbf{v}^{\pm}(y), \tag{32}$$

where I is the identity matrix. The boundary conditions (29) can be written as

$$\frac{\mathrm{d}\mathbf{w}^{\pm}(y_{\pm})}{\mathrm{d}y}-S^{\pm}\mathbf{w}^{\pm}(y_{\pm})=\boldsymbol{\rho}^{\pm}. \tag{33}$$

The continuity conditions (30) and (31) can be written as

$$\mathbf{w}^+(0)-\mathbf{w}^-(0)=0, \tag{34}$$

and

$$\frac{\mathrm{d}\mathbf{w}^+(0)}{\mathrm{d}y}-\frac{\mathrm{d}\mathbf{w}^-(0)}{\mathrm{d}y}=\mathbf{h}. \tag{35}$$

Hence the one-dimensional two-point boundary value problem (18)–(21) is formulated as a *coupled* infinite system (32)–(35).

Lemma 4.2. *For any real polynomials $g_1(\xi)$ and $g_2(\xi)$, it holds*

$$\sum_{k=0}^{\infty} \int_{\mathbb{R}^2} g_1(\xi) g_2(\eta) \psi_i(\xi) \psi_k(\xi) \psi_k(\eta) \psi_j(\eta) \mathrm{d}\xi \, \mathrm{d}\eta = \int_{\mathbb{R}} g_1(\xi) g_2(\xi) \psi_i(\xi) \psi_j(\xi) \mathrm{d}\xi, \quad i, j \geq 0. \tag{36}$$

Proof. We prove this lemma by the method of induction. First, without loss of generality, we may assume g_1 is a constant function, e.g., $g_1 = 1$. By the orthogonality of the Hermite basis functions, we have

$$\sum_{k=0}^{\infty} \int_{\mathbb{R}^2} g_1(\xi) g_2(\eta) \psi_i(\xi) \psi_k(\xi) \psi_k(\eta) \psi_j(\eta) \mathrm{d}\xi \, \mathrm{d}\eta = \sum_{k=0}^{\infty} \int_{\mathbb{R}} g_2(\eta) \psi_k(\eta) \psi_j(\eta) \mathrm{d}\eta \int_{\mathbb{R}} \psi_i(\xi) \psi_k(\xi) \mathrm{d}\xi$$

$$= \int_{\mathbb{R}} g_1(\eta) g_2(\eta) \psi_i(\eta) \psi_j(\eta) \mathrm{d}\eta.$$

Next we show that it holds for $g_1(\xi) = \xi$. Using the recursion (26) and the orthogonality of the Hermite basis functions yield

$$\sum_{k=0}^{\infty} \int_{\mathbb{R}^2} g_1(\xi) g_2(\eta) \psi_i(\xi) \psi_k(\xi) \psi_k(\eta) \psi_j(\eta) \mathrm{d}\xi \, \mathrm{d}\eta$$

$$= \sum_{k=0}^{\infty} \int_{\mathbb{R}} g_2(\eta) \psi_k(\eta) \psi_j(\eta) \mathrm{d}\eta \int_{\mathbb{R}} \xi \psi_i(\xi) \psi_k(\xi) \mathrm{d}\xi$$

$$= \sum_{k=0}^{\infty} \int_{\mathbb{R}} g_2(\eta) \psi_k(\eta) \psi_j(\eta) \mathrm{d}\eta \int_{\mathbb{R}} \left(\sqrt{\frac{i+1}{2}} \psi_{i+1}(\xi) + \sqrt{\frac{i}{2}} \psi_{i-1}(\xi) \right) \psi_k(\xi) \mathrm{d}\xi$$

$$= \int_{\mathbb{R}} g_2(\eta) \left(\sqrt{\frac{i+1}{2}} \psi_{i+1}(\eta) + \sqrt{\frac{i}{2}} \psi_{i-1}(\eta) \right) \psi_j(\eta) \mathrm{d}\eta$$

$$= \int_{\mathbb{R}} g_2(\eta) \eta \psi_i(\eta) \psi_j(\eta) \mathrm{d}\eta = \int_{\mathbb{R}} g_1(\eta) g_2(\eta) \psi_i(\eta) \psi_j(\eta) \mathrm{d}\eta.$$

Now we may assume that it holds for any polynomial $g_1(\xi)$ with degree less than or equal to n. It suffices to show that it holds for any polynomial $g_1(\xi)$ with degree $n+1$. Here we can assume $g_1(\xi)$ has no constant term since (36) is proved for any constant function of g_1. Then we can write $g_1(\xi) = \xi f(\xi)$, where $f(\xi)$ is a polynomial of degree n.

Using the recursion (26) and the orthogonality of the Hermite basis functions again, we have

$$\sum_{k=0}^{\infty} \int_{\mathbb{R}^2} g_1(\xi) g_2(\eta) \psi_i(\xi) \psi_k(\xi) \psi_k(\eta) \psi_j(\eta) \mathrm{d}\xi \, \mathrm{d}\eta$$

$$= \sum_{k=0}^{\infty} \int_{\mathbb{R}} g_2(\eta) \psi_k(\eta) \psi_j(\eta) \mathrm{d}\eta \int_{\mathbb{R}} f(\xi) \xi \psi_i(\xi) \psi_k(\xi) \mathrm{d}\xi$$

$$= \sum_{k=0}^{\infty} \int_{\mathbb{R}} g_2(\eta) \psi_k(\eta) \psi_j(\eta) \mathrm{d}\eta \int_{\mathbb{R}} f(\xi) \left(\sqrt{\frac{i+1}{2}} \psi_{i+1}(\xi) + \sqrt{\frac{i}{2}} \psi_{i-1}(\xi) \right) \psi_k(\xi) \mathrm{d}\xi$$

$$= \sum_{k=0}^{\infty} \sqrt{\frac{i+1}{2}} \int_{\mathbb{R}^2} f(\eta) g_2(\xi) \psi_{i+1}(\xi) \psi_k(\xi) \psi_k(\eta) \psi_j(\eta) \mathrm{d}\xi \, \mathrm{d}\eta$$

$$+ \sum_{k=0}^{\infty} \sqrt{\frac{i}{2}} \int_{\mathbb{R}^2} f(\eta) g_2(\xi) \psi_{i-1}(\xi) \psi_k(\xi) \psi_k(\eta) \psi_j(\eta) \mathrm{d}\xi \, \mathrm{d}\eta$$

$$= \sqrt{\frac{i+1}{2}} \int_{\mathbb{R}} f(\eta) g_2(\eta) \psi_{i+1}(\eta) \psi_j(\eta) \mathrm{d}\eta + \sqrt{\frac{i}{2}} \int_{\mathbb{R}} f(\eta) g_2(\eta) \psi_{i-1}(\eta) \psi_j(\eta) \mathrm{d}\eta$$

$$= \int_{\mathbb{R}} g_2(\eta) f(\eta) \left(\sqrt{\frac{i+1}{2}} \psi_{i+1}(\eta) + \sqrt{\frac{i}{2}} \psi_{i-1}(\eta) \right) \psi_j(\eta) \mathrm{d}\eta$$

$$= \int_{\mathbb{R}} g_2(\eta) f(\eta) \eta \psi_i(\eta) \psi_j(\eta) \mathrm{d}\eta = \int_{\mathbb{R}} g_2(\eta) g_1(\eta) \psi_i(\eta) \psi_j(\eta) \mathrm{d}\eta,$$

which completes the proof. □

Denote by $\langle \cdot, \cdot \rangle$ and $(\cdot, \cdot)$ the inner products in l^2 and L^2, respectively. Let $\mathbf{u} = [u_0, u_1, \ldots]^\top, \mathbf{v} = [v_0, v_1, \ldots]^\top \in l^2$, and

$$u(x) = \sum_{k=0}^{\infty} u_k \psi_k(x) \quad \text{and} \quad v(x) = \sum_{k=0}^{\infty} u_k \psi_k(x).$$

Lemma 4.3. *For any integer $k \geq 0$, it holds*

$$\langle A^k \mathbf{u}, \mathbf{v} \rangle = \left(x^{2k} u(x), v(x) \right). \tag{37}$$

Proof. We prove this lemma by the method of induction. Clearly, it follows from the definitions of the inner products in l^2 and L^2 that the identity (37) is satisfied, i.e.,

$$\langle \mathbf{u}, \mathbf{v} \rangle = \left(u(x), v(x) \right).$$

So, we first prove that the identity (37) is satisfied for $k = 1$. It follows from the definitions that we have

$$\left(x^2 u(x), v(x) \right) = \left(x^2 \sum_{i=0}^{\infty} u_i \psi_i(x), \sum_{j=0}^{\infty} v_j \psi_j(x) \right) = \sum_{i=0}^{\infty} \sum_{j=0}^{\infty} u_i v_j \left(x^2 \psi_i(x), \psi_j(x) \right) = \sum_{i=0}^{\infty} \sum_{j=0}^{\infty} u_i v_j a_{ji} = \langle A \mathbf{u}, \mathbf{v} \rangle.$$

We assume that (37) is satisfied for some integer $k > 1$, i.e.,

$$\langle A^k \mathbf{u}, \mathbf{v} \rangle = \left(x^{2k} u(x), v(x) \right).$$

Next we show that (37) is satisfied for the integer $k + 1$. Using Lemma 4.2, we have

$$\left(x^{2(k+1)} u(x), v(x) \right) = \left(x^2 \left(x^{2k} u(x) \right), v(x) \right) = \sum_{i=0}^{\infty} \sum_{j=0}^{\infty} u_i v_j \left(x^2 x^{2k} \psi_i(x), \psi_j(x) \right)$$

$$= \sum_{i=0}^{\infty} \sum_{j=0}^{\infty} u_i v_j \sum_{m=0}^{\infty} \left(x^2 \psi_i(x), \psi_m(x) \right) \left(x^{2k} \psi_m(x), \psi_j(x) \right) = \sum_{i=0}^{\infty} \sum_{j=0}^{\infty} u_i v_j \sum_{m=0}^{\infty} a_{mi} \langle A^k \mathbf{e}_m, \mathbf{e}_j \rangle$$

$$= \sum_{m=0}^{\infty} \left(\sum_{i=0}^{\infty} u_i a_{mi} \right) \left(\sum_{j=0}^{\infty} v_j \langle A^k \mathbf{e}_m, \mathbf{e}_j \rangle \right) = \sum_{m=0}^{\infty} (A\mathbf{u})_m \langle A^k \mathbf{e}_m, \mathbf{v} \rangle$$

$$= \left\langle A^k \sum_{m=0}^{\infty} (A\mathbf{u})_m \mathbf{e}_m, \mathbf{v} \right\rangle = \langle A^k A \mathbf{u}, \mathbf{v} \rangle = \langle A^{k+1} \mathbf{u}, \mathbf{v} \rangle,$$

where $\mathbf{e}_m$ is the unit vector, whose mth component is one and others are zeros. □

Lemma 4.4. *The matrices $S^\pm$ can be expressed as*

$$S^\pm = \sum_{k=0}^{\infty} \frac{g_\pm^{(k)}(0)}{k!} A^k,$$

where $g_\pm(\xi) = \mathrm{i} \sqrt{\kappa_\pm^2 - \xi}$.

Proof. Since $\kappa_\pm$ are complex numbers and $g_\pm(\xi)$ are analytic on the whole real axis, we have the Maclaurin series expansions for $g_\pm(\xi)$:

$$g_\pm(\xi) = \sum_{k=0}^{\infty} \frac{g_\pm^{(k)}(0)}{n!} \xi^k \quad \text{for all real } \xi. \tag{38}$$

It follows from (37) that we have

$$\langle S^{\pm}\mathbf{e}_j, \mathbf{e}_i\rangle = \left(g_{\pm}\left(\xi^2\right)\psi_j(\xi), \psi_i(\xi)\right) = \left(\sum_{k=0}^{\infty}\frac{g_{\pm}^{(k)}(0)}{k!}\left(\xi^{2k}\right)\psi_j(\xi), \psi_i(\xi)\right)$$

$$= \sum_{k=0}^{\infty}\frac{g_{\pm}^{(k)}(0)}{k!}\left(\xi^{2k}\psi_j(\xi), \psi_i(\xi)\right)$$

$$= \sum_{k=0}^{\infty}\frac{g_{\pm}^{(k)}(0)}{k!}\langle A^k\mathbf{e}_j, \mathbf{e}_i\rangle = \left\langle \sum_{k=0}^{\infty}\frac{g_{\pm}^{(k)}(0)}{k!}A^k\mathbf{e}_j, \mathbf{e}_i\right\rangle,$$

which completes the proof. $\square$

As a direct consequence of Lemma 4.4, we have

Theorem 4.1. *The matrices A and $S^{\pm}$ commute, i.e.,*

$$AS^{\pm} = S^{\pm}A. \tag{39}$$

This theorem implies that A and $S^{\pm}$ can be simultaneously diagonalized, and consequently, the system (32)–(35) can be *decoupled*.

4.2. Finite dimensional approximation

We now construct a finite dimensional approximation to the system (32)–(35) which can be decoupled by simultaneous diagonalization. We note that while the infinite matrices A and $S^{\pm}$ commute (cf. (39)), a direct truncation does not preserve the commutativity (cf. Remark 4.1) which is essential for the decoupling.

Define a finite dimensional subspace of $L^2(\mathbb{R})$:

$$X_M = \text{span}\{\psi_0, \psi_1, \ldots, \psi_M\}.$$

Numerically, we shall seek the solution in the finite dimensional subspace X_M. We assume that the numerical solution has the expansion

$$w_M^{\pm}(x, y) = \sum_{m=0}^{M} w_m^{\pm}(y)\psi_m(x).$$

Define a diagonal matrix

$$D_M = \text{diag}\left((-i)^0, (-i)^1, (-i)^2, \ldots, (-i)^M\right)$$

and vectors

$$\mathbf{w}_M^{\pm}(y) = D_M \cdot \left(w_0^{\pm}(y), w_1^{\pm}(y), \ldots, w_M^{\pm}(y)\right)^{\top},$$

$$\mathbf{v}_M^{\pm}(y) = D_M \cdot \left(v_0^{\pm}(y), v_1^{\pm}(y), \ldots, v_M^{\pm}(y)\right)^{\top},$$

$$\boldsymbol{\rho}_M^{\pm} = D_N \cdot \left(\rho_0^{\pm}, \rho_1^{\pm}, \ldots, \rho_M^{\pm}\right)^{\top},$$

$$\mathbf{h}_M = D_M \cdot \left(h_1, h_2, \ldots, h_M\right)^{\top}.$$

Denote by $A_M = (a_{ij})_{0\leq i,j\leq M}$ the truncation of the matrix A. Define

$$S_M^{\pm} = \sum_{k=0}^{\infty}\frac{g_{\pm}^{(k)}(0)}{k!}(A_M)^k. \tag{40}$$

Remark 4.1. The matrices $S_M^{\pm}$ are not simply the truncation of the matrices $S^{\pm}$ given by

$$\left(S^{\pm}\right)_M = \sum_{k=0}^{\infty}\frac{g_{\pm}^{(k)}(0)}{k!}\left(A^k\right)_M.$$

However, the difference between $S_M^{\pm}$ and $(S^{\pm})_M$ are high order terms which converge to zero as M increases.

The finite dimensional approximation to (32)–(35) is

$$\frac{d^2 \mathbf{w}_M^\pm(y)}{dy^2} + \left(\kappa_\pm^2 I_M - A_M\right)\mathbf{w}_M^\pm(y) = \mathbf{v}_M^\pm(y),$$

(41)

with the boundary conditions

$$\frac{d\mathbf{w}_M^\pm(y_\pm)}{dy} - S_M^\pm \mathbf{w}_M^\pm(y_\pm) = \boldsymbol{\rho}_M^\pm,$$

(42)

and the continuity conditions

$$\mathbf{w}_M^+(0) - \mathbf{w}_M^-(0) = 0,$$

(43)

and

$$\frac{d\mathbf{w}_M^+(0)}{dy} - \frac{d\mathbf{w}_M^-(0)}{dy} = \mathbf{h}_M.$$

(44)

The above system of $(M + 1)$ equations is *coupled* together by the matrices A_M and $S_M^\pm$.

Theorem 4.2. *The matrices A_M and $S_M^\pm$ are simultaneously diagonalizable. Moreover, let $\{\lambda_j\}_{0 \le j \le M}$ be the set of eigenvalues of A_M, then the eigenvalues of $S_M^\pm$ are given by*

$$\sigma_j^\pm = i\sqrt{\kappa_\pm^2 - \lambda_j}, \quad 0 \le j \le M.$$

(45)

Proof. By definition, A_M is a real symmetric matrix. Hence, there exists an $M \times M$ orthonormal matrix Q_M such that

$$Q_M^\top A_M Q_M = \Lambda_M,$$

where Λ_M is an $M \times M$ diagonal matrix.

It follows from the definitions of $S_M^\pm$ that we have

$$Q_M^\top S_M^\pm Q_M = \sum_{k=0}^\infty \frac{g_\pm^{(k)}(0)}{k!} Q_M^\top (A_M)^k Q_M = \sum_{k=0}^\infty \frac{g_\pm^{(k)}(0)}{k!} \left(Q_M^\top A_M Q_M\right)^k$$

$$= \sum_{k=0}^\infty \frac{g_\pm^{(k)}(0)}{k!} \Lambda_M^k := \Sigma_M^\pm = \text{diag}\{\sigma_0^\pm, \sigma_1^\pm, \cdots, \sigma_M^\pm\},$$

(46)

which completes the proof. □

By Theorem 4.2, the matrices $S_M^\pm$ and A_M can be simultaneously diagonalized by the same orthogonal matrix Q_M, i.e., there exist an orthonormal matrix Q_M and two $M \times M$ diagonal matrices Λ_M and Σ_M such that

$$Q_M^\top A_M Q_M = \Lambda_M \quad \text{and} \quad Q_M^\top S_M^\pm Q_M = \Sigma_M^\pm.$$

Denote $\tilde{\mathbf{w}}_M^\pm(y) = Q_M^\top \mathbf{w}_M^\pm(y)$, $\tilde{\mathbf{v}}_M^\pm(y) = Q_M^\top \mathbf{v}_M^\pm(y)$, $\tilde{\boldsymbol{\rho}}_M^\pm = Q_M^\top \boldsymbol{\rho}_M^\pm$, $\tilde{\mathbf{h}}_M = Q_M^\top \mathbf{h}_M$. Multiplying $Q_M^\top$ on both sides of (41) and using the simultaneous diagonalization property, we deduce a fully decoupled system of $M + 1$ equations:

$$\frac{d^2 \tilde{\mathbf{w}}_M^\pm(y)}{dy^2} + \left(\kappa_\pm^2 I_M - \Lambda_M\right)\tilde{\mathbf{w}}_M^\pm(y) = \tilde{\mathbf{v}}_M^\pm(y),$$

(47)

with the boundary conditions

$$\frac{d\tilde{\mathbf{w}}_M^\pm(y_\pm)}{dy} - \Sigma_M^\pm \tilde{\mathbf{w}}_M^\pm(y_\pm) = \tilde{\boldsymbol{\rho}}_M^\pm,$$

(48)

and the continuity conditions

$$\tilde{\mathbf{w}}_M^+(0) - \tilde{\mathbf{w}}_M^-(0) = 0,$$

(49)

and

$$\frac{d\tilde{\mathbf{w}}_M^+(0)}{dy} - \frac{d\tilde{\mathbf{w}}_M^-(0)}{dy} = \tilde{\mathbf{h}}_M.$$

(50)

Once $\tilde{\mathbf{w}}_M^\pm$ is obtained by solving the above decoupled two-point boundary value problem (47)–(50), we can compute $\mathbf{w}_M^\pm = Q_M \tilde{\mathbf{w}}_M^\pm$.

Remark 4.2. In practice, it is not required to generate the matrix $S_M^\pm$ explicitly since all we need is the diagonal matrix $\Sigma_M^\pm$ whose elements can be computed directly by using (45).

4.3. Legendre–Galerkin approximation

The problem (47)–(50) consists of a sequence of decoupled two-point boundary value problem which can be solved, for example, by the Legendre–Galerkin method [32]. In this section, we briefly discuss the Legendre–Galerkin method to solve the following two-point boundary value model problem, and refer to the book [33] for more detail.

Consider the second-order ordinary differential equation

$$\frac{d^2 u^\pm(y)}{dy^2} + \eta^\pm u^\pm(y) = v^\pm(y), \tag{51}$$

together with the boundary conditions on $y = y^\pm$

$$\frac{du^\pm(y^\pm)}{dy} - \sigma^\pm u^\pm(y^\pm) = \rho^\pm, \tag{52}$$

and the continuity conditions

$$u^+(0) - u^-(0) = 0, \tag{53}$$

$$\frac{du^+(0)}{dy} - \frac{du^-(0)}{dy} = h. \tag{54}$$

The above one-dimensional transmission problem (51)–(54) is exactly the same as the one studied in [21], and can be efficiently solved by using a Legendre–Galerkin method (cf. [32]) which is described in detail in Section 4 of [21]. With a suitable choice of basis functions, the Legendre–Galerkin method leads to a sequence of sparse linear system which can be inverted in $O(N)$ operations, where N is the number of unknowns in the Legendre expansion.

4.4. Algorithm and complexity

Given the problem parameters: wave numbers (κ_+, κ_-), surface perturbation ε, we choose the numerical parameters: M to be the number of Hermite expansion in the horizontal x direction, N to be the number of Legendre expansion in the vertical y direction, and K to be the number of Taylor expansion retained in the perturbation expansion. The numerical solution can be written in the following form:

$$u^\pm(x, y) = \sum_{m=0}^{M} \sum_{n=0}^{N} \sum_{k=0}^{K} w_{m,n,k}^\pm \psi_m(x) \phi_n^\pm(y) \varepsilon^k. \tag{55}$$

Therefore, the numerical algorithm is to compute the coefficients set $\{w_{m,n,k}^\pm\}$ for $m = 0, ..., M$, $n = 0, ..., N$, and $k = 0, ..., K$, which can be summarized as follows:

Pre-computation: (independent of wavenumbers $\kappa_\pm$)

1. Compute the Hermite Gauss points $\{x_n\}_{n=0,...,M}$, Legendre–Gaussian–Lobatto collocation points $\{y_n^+\}_{n=0,...,N}$ on interval $[0, y^+]$ and $\{y_n^-\}_{n=0,...,N}$ on interval $[y^-, 0]$. ($O(N) + O(M)$ flops.)
2. Compute the matrix A_M, and its eigenpair (Q_M, Λ_M). ($O(M^2)$ flops.)

Then, for each incident wave:

1. Compute $\Sigma_M^\pm$ through (45);
2. **for** $k = 1 : K$ **do**
       for $m = 1 : M$ **do**
         Solve each one dimensional problem to obtain $\{w_{m,n,k}^\pm\}$ for $n = 0, ..., N$
       end for
     end for
3. Calculate $u^\pm(x, y)$ through (55).

The computational complexity for each k in Step 2 is of order $O(M^2 N) + O(MN^2)$ which comes from the matrix–matrix multiplications involving the eigenmatrix Q_M and also comes from applying the discrete Legendre transforms and discrete Hermite transforms [33]. Hence, the total computational complexity is of order $O(M^2 NK) + O(MN^2 K)$.

5. Numerical experiments

In this section, we present some numerical experiments to demonstrate the efficiency and accuracy of the proposed method. Two cases are considered; one is a plane surface scattering, where the analytic solution is available and can be used for accuracy test of the numerical solution, and another is rough surface scattering. The code was written in Matlab and the computations were run on an Intel Core i5 processor (1.7 GHz, 4 GB 1333 MHz DDR3 memory).

5.1. Plane surface scattering

In [23], the fundamental solution is introduced for the two-dimensional Helmholtz equation in a two-layered medium. For the observation point $\mathbf{r} = (x, y)$ and source point $\mathbf{r}' = (x', y')$, the fundamental solution of Helmholtz equation in a two-layered background medium in $\mathbb{R}^2$ satisfies

$$\Delta G(\mathbf{r}, \mathbf{r}') + \kappa^2(\mathbf{r}) G(\mathbf{r}, \mathbf{r}') = -\delta(\mathbf{r} - \mathbf{r}'),$$

with continuity conditions on the interface

$$G(\mathbf{r}, \mathbf{r}')\big|_{y=0^+} = G(\mathbf{r}, \mathbf{r}')\big|_{y=0^-}$$
$$\partial_y G(\mathbf{r}, \mathbf{r}')\big|_{y=0^+} = \partial_y G(\mathbf{r}, \mathbf{r}')\big|_{y=0^-},$$

where the wavenumber

$$\kappa(\mathbf{r}) = \begin{cases} \kappa_1 & \text{for } y > 0, \\ \kappa_2 & \text{for } y < 0. \end{cases}$$

Denote $\beta_i^2 = \kappa_i^2 - \xi^2$ with $\text{Im}\,\beta_i \geq 0$. It follows from the Fourier transform that the fundamental solution is given by

$$G(\mathbf{r}, \mathbf{r}') = \begin{cases} \Psi^{(1)}(\mathbf{r}, \mathbf{r}') + \Phi_1(\mathbf{r}, \mathbf{r}') & \text{for } y > 0, \ y' > 0, \\ \Psi^{(2)}(\mathbf{r}, \mathbf{r}') + \Phi_2(\mathbf{r}, \mathbf{r}') & \text{for } y < 0, \ y' < 0, \\ \Psi^{(3)}(\mathbf{r}, \mathbf{r}') & \text{for } y > 0, \ y' < 0, \\ \Psi^{(4)}(\mathbf{r}, \mathbf{r}') & \text{for } y < 0, \ y' > 0, \end{cases}$$

where

$$\Psi^{(1)}(\mathbf{r}, \mathbf{r}') = \frac{\mathrm{i}}{4\pi} \int_{-\infty}^{\infty} \frac{1}{\beta_1} \frac{\beta_1 - \beta_2}{\beta_1 + \beta_2} e^{\mathrm{i}\beta_1(y+y')} e^{\mathrm{i}\xi(x-x')} \mathrm{d}\xi,$$

$$\Psi^{(2)}(\mathbf{r}, \mathbf{r}') = \frac{\mathrm{i}}{4\pi} \int_{-\infty}^{\infty} \frac{1}{\beta_2} \frac{\beta_2 - \beta_1}{\beta_1 + \beta_2} e^{-\mathrm{i}\beta_2(y+y')} e^{\mathrm{i}\xi(x-x')} \mathrm{d}\xi,$$

$$\Psi^{(3)}(\mathbf{r}, \mathbf{r}') = \frac{\mathrm{i}}{2\pi} \int_{-\infty}^{\infty} \frac{e^{\mathrm{i}(\beta_1 y - \beta_2 y')}}{\beta_1 + \beta_2} e^{\mathrm{i}\xi(x-x')} \mathrm{d}\xi,$$

$$\Psi^{(4)}(\mathbf{r}, \mathbf{r}') = \frac{\mathrm{i}}{2\pi} \int_{-\infty}^{\infty} \frac{e^{\mathrm{i}(\beta_1 y - \beta_2 y')}}{\beta_1 + \beta_2} e^{\mathrm{i}\xi(x-x')} \mathrm{d}\xi,$$

and Φ_i is the fundamental solution of the Helmholtz equation in homogeneous background medium in $\mathbb{R}^2$ with wavenumber κ_i, i.e.,

$$\Phi_i(\mathbf{r}, \mathbf{r}') = \frac{\mathrm{i}}{4} H_0^{(1)}(\kappa_i |\mathbf{r} - \mathbf{r}'|), \quad i = 1, 2.$$

We consider the case where the surface is a plane, i.e., $f(x) = 0$. We can compare numerical solution with the analytic solution given above. Recall that the point (x_0, y_0) is where the source is placed. In this section, we always assume the point source is placed at $(x_0, y_0) = (0.0, 1.5)$ and the transparent boundaries are put at $y^+ = 1$ and $y^- = -1$.

First, we investigate the convergence of the series solution in the horizontal x-direction. We fix $N = 40$ and vary M with four different wavenumber cases:

Case 1: $(\kappa_+, \kappa_-) = (10.5 + 1.0\mathrm{i}, 20.5 + 1.0\mathrm{i})$,

Case 2: $(\kappa_+, \kappa_-) = (1.5 + 1.0\mathrm{i}, 2.5 + 1.0\mathrm{i})$,

Case 3: $(\kappa_+, \kappa_-) = (10.5 + 0.5\mathrm{i}, 20.5 + 0.5\mathrm{i})$,

Case 4: $(\kappa_+, \kappa_-) = (1.5 + 0.5\mathrm{i}, 2.5 + 0.5\mathrm{i})$.

The results are shown in Fig. 2 (left) and in Fig. 3 (left), which plot the $L^2(\Omega)$ error and the CPU time of the numerical solution again the number of truncation in the x-direction M, respectively. It can be seen from the results that the numerical solutions converge exponentially as M is increased and the computational time is consistent with our theoretical computational complexity. We point out that the wavenumbers with large real and small imaginary values require much larger M in order to maintain the same order of accuracy. However, for those wavenumber with either big real and imaginary values
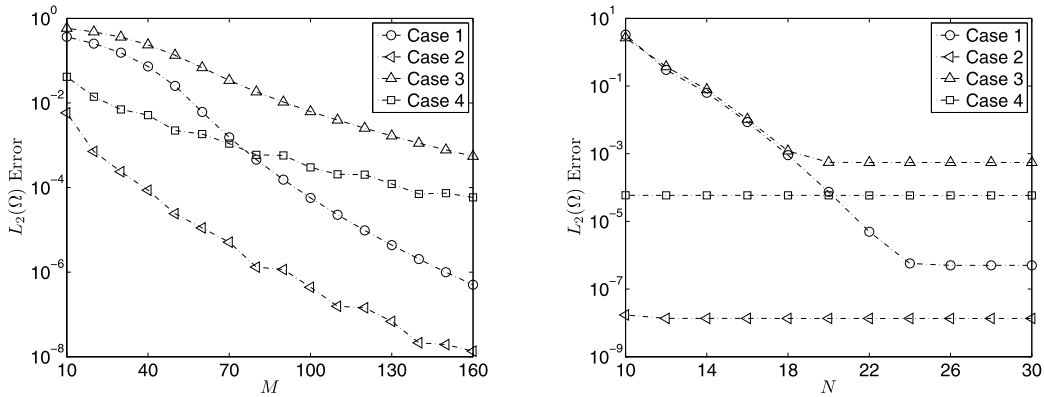
Fig. 2. The $L^2(\Omega)$ error of the numerical solution is plotted against the number of truncation terms for flat surface scattering. (Left) The error is plotted against the truncation term in the horizontal x-direction M; (right) the error is plotted against the truncation term in the vertical y-direction N.
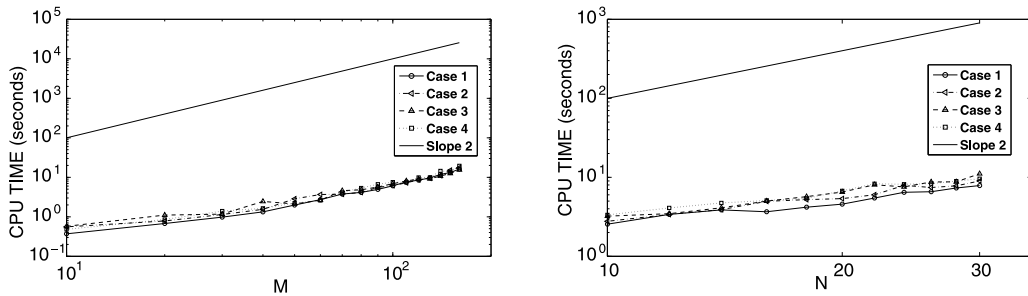
Fig. 3. The CPU time is plotted against the number of truncation terms for flat surface scattering. (left) The CPU is plotted against the truncation term in the horizontal x-direction M; (right) The CPU is plotted against the truncation term in the vertical y-direction N.

or small real and imaginary values, e.g., Case 1 and Case 4, the impact of the imaginary value of the wavenumber will eventually affect the numerical accuracy.

Next, we investigate the convergence of the series solution in vertical y-direction. In this test, we only vary the parameter N, and take a sufficiently large M, e.g., $M = 160$, such that the approximation error is negligibly small in the x-direction. We consider the same four cases as the previous investigation. The results are shown in Fig. 2 (right) and in Fig. 3 (right), which plot the $L^2(\Omega)$ error and the CPU time of the numerical solution against the number of truncation in the y-direction N. Again, we notice an exponential convergence as N is increased and the consistence of the actual CPU time with the theoretical computational complexity. It is clear to note that the wavenumbers with large real and small imaginary values require much larger N to reach the same level of accuracy. Similarly, for the wavenumbers with either big real and imaginary values or small real and imaginary values, e.g., Case 1 and Case 4, the impact of the imaginary value of the wavenumber will eventually affect the numerical accuracy.

Finally, we investigate the convergence of the series solution with respect to the wavenumber. We fix the real part of $\kappa_\pm$, e.g., $\mathrm{Re}(\kappa_+) = 1.5$ and $\mathrm{Re}(\kappa_-) = 2.5$, and vary both of the imaginary parts of $\kappa_\pm$ from 0.1 to 1. The results are displayed in Fig. 4 (left) for fixed $M = 200$ and $N = 80$. Then we fix the imaginary part of $\kappa_\pm$, e.g., $\mathrm{Im}(\kappa_+) = 1$ and $\mathrm{Im}(\kappa_-) = 1$, and vary both of the real parts of $\kappa_\pm$ from $\mathrm{Re}(\kappa_+) = 1$ to 20 and $\mathrm{Re}(\kappa_-) = 2\mathrm{Re}(\kappa_+)$. The result are displayed in Fig. 4 (right) with fixed truncation terms $M = 200$ and $N = 80$. As expected, the error decreases as the imaginary part of the wavenumber increases, while the error increases as the real part of the wavenumber increases.

5.2. Rough surface scattering

In this subsection, we investigate the case of rough surface scattering and determine how the numerical accuracy depends on the parameter K, i.e., the term in the series solution. We fix the parameters M and N such that the approximation error is negligibly small in terms of M and N. To test the convergence of the method, we denote a relative $L^2(\Omega)$ error:

$$\mathrm{E}_K = \frac{\|u_K - u_{K-1}\|_{L^2(\Omega)}}{\|u_K\|_{L^2(\Omega)}}.$$

First, we consider Case 2, i.e., $(\kappa^+, \kappa^-) = (1.5 + 1.0i, 2.5 + 1.0i)$ and choose the function $g_1(x) = \cos(x)$ to represent the rough surface. We fix $\varepsilon = 0.1$, $M = 100$, $N = 30$, and vary K from 1 to 16. The convergent result is shown in the column of Test 1 in Table 1. We also change ε from 0.2 to 0.8. The convergent results with respect to different ε are displayed in Fig. 5,
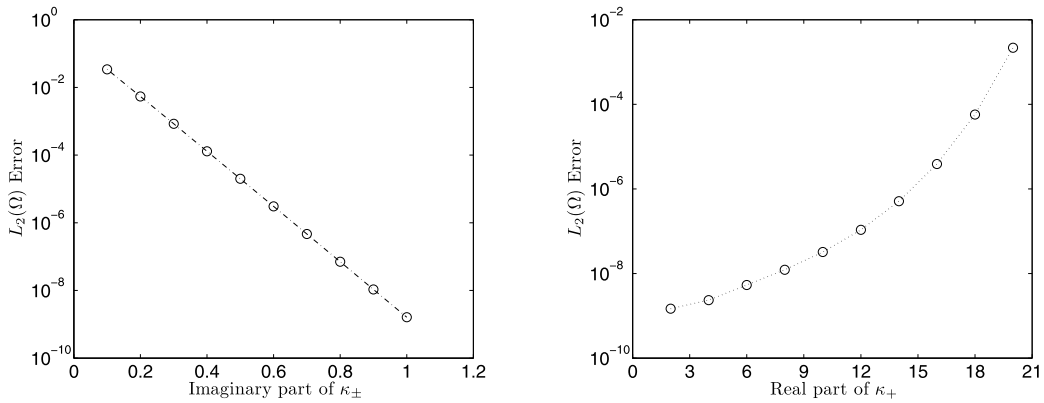
Fig. 4. The $L^2(\Omega)$ error of the numerical solution is plotted against the wavenumbers for flat surface scattering. (Left) The error is plotted against the real parts of the wavenumbers; (right) the error is plotted against the imaginary parts of the wavenumbers.

Table 1
Convergence test for different wavenumbers and perturbation parameter ε for rough surface scattering.

| K	Test 1	Test 2	Test 3	Test 4
1	1.0E+00	1.0E+00	1.0E+00	1.0E+00
2	1.09E−01	5.71E−01	8.68E−02	6.07E−01
3	1.14E−02	3.03E−01	4.03E−03	3.83E−01
4	8.67E−04	3.56E−01	9.33E−04	3.71E−01
5	1.75E−04	3.74E−01	1.33E−04	1.27E−01
6	2.47E−05	9.12E−02	1.00E−05	1.87E−01
7	7.31E−07	8.15E−02	3.73E−07	9.91E−02
8	1.14E−07	1.01E−01	1.15E−07	9.27E−02
9	2.51E−08	3.29E−02	1.00E−08	6.64E−02
10	2.69E−09	3.64E−02	6.76E−10	3.22E−02
11	1.41E−10	5.20E−02	1.28E−10	3.89E−02
12	2.91E−11	2.80E−02	1.58E−11	1.57E−02
13	4.11E−12	1.03E−02	8.80E−13	1.99E−02
14	2.93E−13	2.18E−02	1.51E−13	1.25E−02
15	1.70E−14	1.56E−02	2.40E−14	8.52E−03
16	5.01E−15	4.49E−03	2.00E−15	8.26E−03
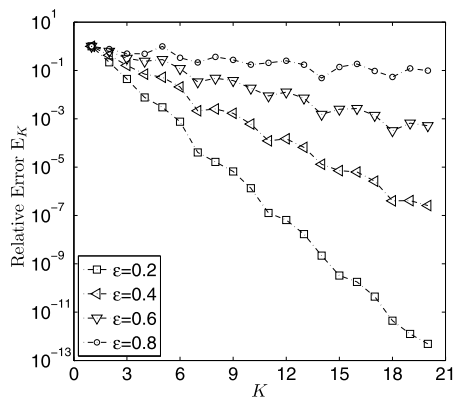
**Fig. 5.** Relative $L^2(\Omega)$ error is plotted against the number of truncation K in the series solution.

which plots the relative $L^2(\Omega)$ error E_K against the number of truncation in the series solution K. It can be observed that the convergence rate highly depends on the value of ε when fixing all the other parameters, and smaller ε leads to faster convergence with a few iterations.

Second, we still consider Case 2, i.e., $(\kappa^+, \kappa^-) = (1.5 + 1.0i, 2.5 + 1.0i)$, choose the same truncation terms $M = 100$ and $N = 30$, and vary K from 1 to 16. We choose the function $g_2(x) = \cos(4x) + 2\cos(2x) + 4\cos(x)$ for the rough surface with two different values of parameter ε: $\varepsilon_1 = 0.1$ and $\varepsilon_2 = 0.1/7$ such that $\max\{\varepsilon_2 g_2(x)\} = 0.1$. The convergent results are displayed in the column Test 2 and Test 3 in Table 1. The convergence for Test 2, corresponding to larger perturbation
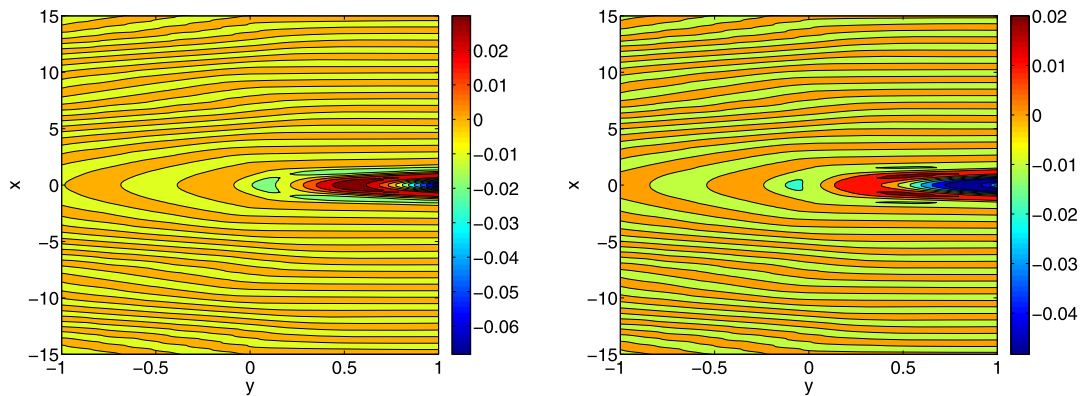
Table 2
Three test examples for rough surface scattering.

Test	(κ^+, κ^-)	ε	$g(x)$	(M, N, K)	CPU time (s)
Case 5	$(1.5 + 1.0i, 2.5 + 1.0i)$	0.1	$g_1(x)$	$(100, 30, 20)$	64.98
Case 6	$(5.5 + 1.0i, 10.5 + 1.0i)$	0.2	$g_1(x)$	$(160, 30, 20)$	181.45
Case 7	$(1.5 + 0.5i, 2.5 + 1.0i)$	0.1	$g_2(x)$	$(150, 40, 20)$	215.11
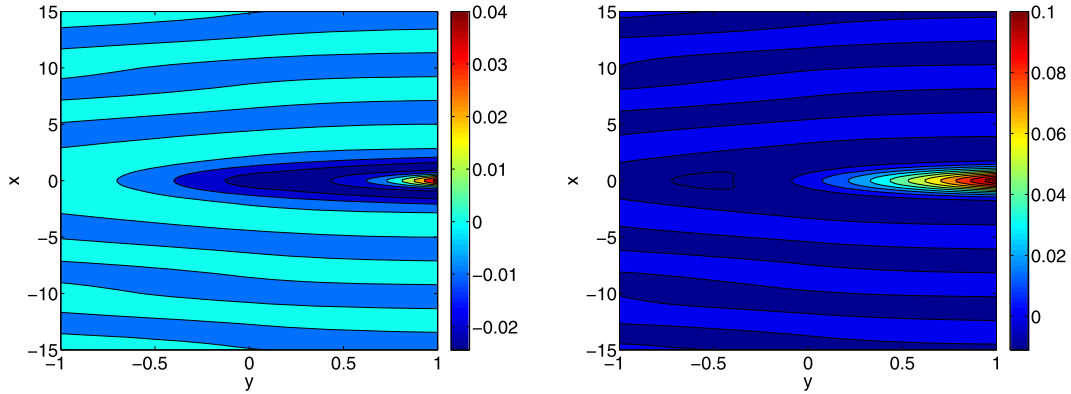
Fig. 6. Contour plot of the total field for Case 5. (Left) Real part of the total field; (right) imaginary part of the total field.

Fig. 7. Contour plot of the total field for Case 6. (Left) Real part of the total field; (right) imaginary part of the total field.

parameter $\varepsilon_1 = 0.1$, is much slower than the convergence for Test 3, corresponding to smaller perturbation parameter $\varepsilon_2 = 0.1/7$.

Next, we consider Case 1, i.e., $(\kappa^+, \kappa^-) = (10.5 + 1.0i, 20.5 + 1.0i)$ for the same $M = 160$, $N = 30$, and vary K from 1 to 16. The rough surface is chosen as $g_1(x) = \cos(x)$ and $\varepsilon = 0.1$. The convergent results are displayed in the column Test 4 in Table 1.

Although we consider the same wave numbers (κ^+, κ^-), parameters (M, N) and the same value of ε but with different profiles $g_1(x)$ and $g_2(x)$, we can observe from those results for Test 1 and Test 2 in Table 1 that the convergence rate of Test 1 is apparently much faster than that of Test 2. The reason is that $\max |g_2(x)|$ is almost seven times of $\max |g_1(x)|$. When we decrease the value of ε to $0.1/7$ in Test 3, we can see that the convergence rate of Test 1 and Test 3 are almost the same as we increase K. Therefore the maximum height of the perturbed profile plays more important role on the convergence of our numerical algorithm than its shape, which is also consistent with the results in Fig. 5. Comparing the results of Test 1 and Test 4, we can observe that Test 4 with large wave numbers converges much slower than Test 1 with small wave numbers. So we can conclude that the value of the wavenumber is also another important factor on the convergence rate.

Finally, we consider three different examples given in Table 2. The contour plot of the total field are displayed in Fig. 6, Fig. 7, and Fig. 8, respectively.
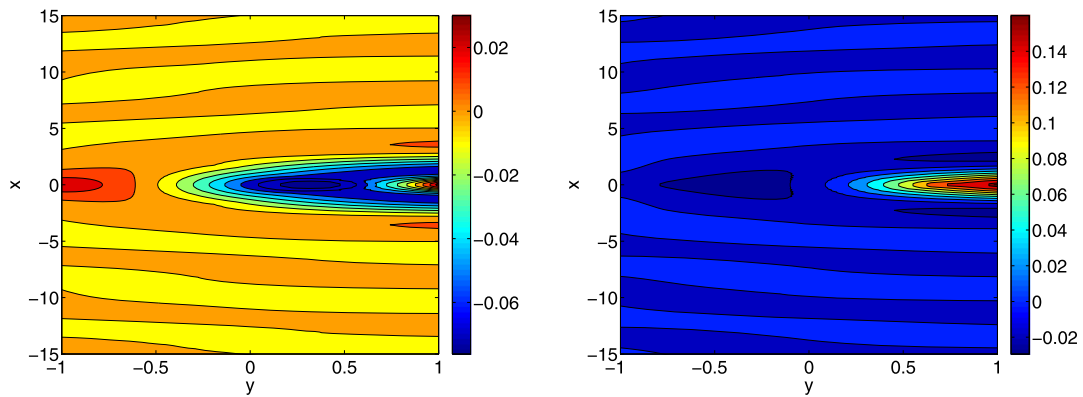
Fig. 8. Contour plot of the total field for Case 7. (Left) Real part of the total field; (right) imaginary part of the total field.

6. Summary

We developed a new spectral method for solving the two-dimensional acoustic wave scattering problem by unbounded rough surfaces. The main difficulty of the problem is that the non-local boundary conditions prevent us from decoupling the two-dimensional system to a sequence of one-dimensional problems with a usual approach. The main novelty of the proposed method is to expand the solution using the Hermite orthonormal basis functions in the Fourier space, and to simultaneously diagonalize the two coupling matrices by using the essential property that the Hermite functions are eigenfunctions of the Fourier transform. The combined approach allows us to reduce the original two-dimensional boundary value problem into a sequence of fully decoupled the one-dimensional Helmholtz equations, with piecewise constant wavenumbers, that can be efficiently solved by using a Legendre–Galerkin method.

We investigated the errors of the numerical solution in terms of the horizontal truncation term M, vertical truncation term N, power series truncation term K, and the wavenumbers $\kappa_\pm$, for both the plane surface scattering and the rough surface scattering. The numerical results indicate that the method is efficient, accurate, and well suited for the unbounded rough surface scattering problem. To the best of our knowledge, this is the first rigorous and robust numerical method for the scattering problem by unbounded rough surfaces.

It is clear that the current approach can be extended to handle the two-dimensional multi-layered unbounded rough surface scattering. We plan to extend the method to the electromagnetic wave scattering by unbounded rough surfaces, where the three-dimensional Maxwell equations have to be considered.

References

[1] T. Arens, T. Hohage, On radiation conditions for rough surface scattering problems, IMA J. Appl. Math. 70 (2005) 839–847.
[2] O. Bruno, F. Reitich, Numerical solution of diffraction problems: a method of variation of boundaries, J. Opt. Soc. Am. A 10 (1993) 1168–1175.
[3] O. Bruno, F. Reitich, Numerical solution of diffraction problems: a method of variation of boundaries. II. Finitely conducting gratings, Padé approximants, and singularities, J. Opt. Soc. Am. A 10 (1993) 2307–2316.
[4] O. Bruno, F. Reitich, Numerical solution of diffraction problems: a method of variation of boundaries. III. Doubly periodic gratings, J. Opt. Soc. Am. A 10 (1993) 2551–2562.
[5] O. Bruno, F. Reitich, Boundary-variation solutions for bounded-obstacle scattering problems in three dimensions, J. Acoust. Soc. Am. 104 (1998) 2579–2583.
[6] O. Bruno, F. Reitich, High-order boundary perturbation methods, in: G. Bao, L. Cowsar, W. Masters (Eds.), Mathematical Modeling in Optical Sciences, in: Frontiers in Applied Mathematics Series, vol. 22, SIAM, Philadelphia, 2001, pp. 71–109.
[7] S.N. Chandler-Wilde, J. Elschner, Variational approach in weighted Sobolev spaces to scattering by unbounded rough surfaces, SIAM J. Math. Anal. 42 (2010) 2554–2580.
[8] S.N. Chandler-Wilde, E. Heinemeyer, R. Potthast, A well-posed integral equation formulating for three-dimensional rough surface scattering, Proc. R. Soc. A 462 (2006) 3683–3705.
[9] S.N. Chandler-Wilde, P. Monk, Existence, uniqueness and variational methods for scattering by unbounded rough surfaces, SIAM J. Math. Anal. 37 (2005) 598–618.
[10] S.N. Chandler-Wilde, P. Monk, M. Thomas, The mathematics of scattering by unbounded, rough, inhomogeneous layers, J. Comput. Appl. Math. 204 (2007) 549–559.
[11] S.N. Chandler-Wilde, C.R. Ross, B. Zhang, Scattering by infinite one-dimensional rough surfaces, Proc. R. Soc. Lond. Ser. A 455 (1999) 3767–3787.
[12] S.N. Chandler-Wilde, B. Zhang, A uniqueness result for scattering by infinite rough surfaces, SIAM J. Appl. Math. 58 (1998) 1774–1790.
[13] D. Courjon, Near-Field Microscopy and Near-Field Optics, Imperial College Press, London, 2003.
[14] J.A. DeSanto, Scattering by rough surfaces, in: R. Pike, P. Sabatier (Eds.), Scattering: Scattering and Inverse Scattering in Pure and Applied Science, Academic Press, New York, 2002, pp. 15–36.
[15] J.A. DeSanto, P.A. Martin, On angular-spectrum representations for scattering by infinite rough surfaces, Wave Motion 24 (1996) 421–433.
[16] J.A. DeSanto, P.A. Martin, On the derivation of boundary integral equations for scattering by an infinite one-dimensional rough surface, J. Acoust. Soc. Am. 102 (1997) 67–77.
[17] J.A. DeSanto, P.A. Martin, On the derivation of boundary integral equations for scattering by an infinite two-dimensional rough surface, J. Math. Phys. 39 (1998) 894–912.

[18] J. Duoandikoetxea, Fourier Analysis, Grad. Stud. Math., vol. 29, American Mathematical Society, 2001.
[19] T.M. Elfouhaily, C.A. Guerin, A critical survey of approximate scattering wave theories from random rough surfaces, Waves Random Media 14 (2004) R1–R40.
[20] Q. Fang, D.P. Nicholls, J. Shen, A stable, high-order method for three-dimensional bounded-obstacle, acoustic scattering, J. Comput. Phys. 224 (2007) 1145–1169.
[21] Y. He, D.P. Nicholls, J. Shen, An efficient and stable spectral method for electromagnetic scattering from a layered periodic structure, J. Comput. Phys. 231 (2012) 3007–3022.
[22] A. Lechleiter, S. Ritterbusch, A variational method for wave scattering from penetrable rough layer, IMA J. Appl. Math. 75 (2010) 366–391.
[23] P. Li, Coupling of finite element and boundary integral method for electromagnetic scattering in a two-layered medium, J. Comput. Phys. 229 (2010) 481–497.
[24] P. Li, H. Wu, W. Zheng, Electromagnetic scattering by unbounded rough surfaces, SIAM J. Math. Anal. 43 (2011) 1205–1231.
[25] P. Li, J. Shen, Analysis of the scattering by an unbounded rough surface, Math. Methods Appl. Sci. 35 (2012) 2166–2184.
[26] D.P. Nicholls, F. Reitich, Shape deformations in rough surface scattering: cancellations, conditioning, and convergence, J. Opt. Soc. Am. A 21 (2004) 590–605.
[27] D.P. Nicholls, F. Reitich, Shape deformations in rough surface scattering: improved algorithms, J. Opt. Soc. Am. A 21 (2004) 606–621.
[28] D.P. Nicholls, J. Shen, A stable high-order method for two-dimensional bounded-obstacle scattering, SIAM J. Sci. Comput. 28 (2006) 1398–1419.
[29] J.A. Ogilvy, Theory of Wave Scattering from Random Rough Surfaces, Adam Hilger, Bristol, 1991.
[30] S. Ritterbusch, Coercivity and the Calderon operator on an unbounded domain, PhD thesis, Karlsruhe Institute of Technology, 2009.
[31] M. Saillard, A. Sentenac, Rigorous solutions for electromagnetic scattering from rough surfaces, Waves Random Media 11 (2001) R103–R137.
[32] J. Shen, Efficient spectral-Galerkin method I. Direct solvers for second-and fourth-order equations by using Legendre polynomials, SIAM J. Sci. Comput. 15 (1994) 1489–1505.
[33] J. Shen, T. Tang, L. Wang, Spectral Methods: Algorithms, Analysis and Applications, in: Springer Series in Computational Mathematics, vol. 41, Springer, 2011.
[34] A.G. Voronovich, Wave Scattering from Rough Surfaces, Springer, Berlin, 1994.
[35] K. Warnick, W.C. Chew, Numerical simulation methods for rough surface scattering, Waves Random Media 11 (2001) R1–R30.
[36] B. Zhang, S.N. Chandler-Wilde, Acoustic scattering by an inhomogeneous layer on a rigid plate, SIAM J. Appl. Math. 58 (1998) 1931–1950.
[37] B. Zhang, S.N. Chandler-Wilde, Integral equation methods for scattering by infinite rough surfaces, Math. Methods Appl. Sci. 26 (2003) 463–488.